DOI: 10.13009/EUCASS2017-438

Solar Concentrator Demonstrator for PocketQubes

Ir. Daniel Martinez Pino, Ir. Barry Zandbergen** and Dr. Ir. Otto Bergsma****
**Chair of Space Systems Engineering, Faculty of Aerospace Engineering, Delft University of Technology*
Kluyverweg 1, 2629HS Delft, The Netherlands
Mail: danielmartinezpino@gmail.com
***Chair of Space Systems Engineering, Faculty of Aerospace Engineering, Delft University of Technology*
Kluyverweg 1, 2629HS Delft, The Netherlands
Phone: +31 152782059, Mail: b.t.c.zandbergen@tudelft.nl
***Chair of Structural Integrity and Composites, Faculty of Aerospace Engineering, Delft University of Technology*
Kluyverweg 1, 2629HS Delft, The Netherlands
Phone: +31152785135, Mail: O.K.Bergsma@tudelft.nl

Abstract
The project we present proposes an inflatable concentrator to mitigate some of the limitations of satellite miniaturisation. The device, tailored for a PocketQube (*PQ*), could be used for Solar Thermal Propulsion (*STP*), communications, electrical power generation and optical systems. In this paper, an iterative design approach is presented, including the optical, thermal and structural modelling as well as the optimisation of the performance and/or the minimisation of the *rms* shape error. It is also discussed the manufacturing and testing of a demonstrator, which allowed to verify and validate the concept, design approach and models developed. Designed with an aperture diameter of about 0.5 m and a packaging volume of 1 *PQ* Unit, the system is able to provide more than 200 W of thermal power. The concentrator shows to be a key enabler for developing a competitive *STP* engine for small satellites.

1. Introduction

The strict constraints imposed by the cost and development time requirements of space missions have been a serious showstopper for engineers and scientists for decades. It is thus understandable that the emergence of pico- and micro-satellites has caused a revolution in the space field, ushering in new opportunities for commercial and scientific missions [1]. Nevertheless, these small satellites are still limited by their size. For instance, the propulsion limitations lead to short lifetimes, the size of their antennae constrain the communication capabilities and the aperture of the optical systems sets a maximum resolution [2].

In the last decade, TU Delft has been actively researching on small satellite technologies [3] [4] and, more specifically, micro propulsion systems [5]. The latter embeds all the research performed on Solar Thermal Propulsion (*STP*) [6], a propulsion technology which uses the solar radiation to heat a propellant up before it is expanded in a thruster to generate the desired thrust [6] [7]. Although *STP* has not been demonstrated, small satellites appear as ideal platforms for the development of this technology thanks to their low cost and short development time. Among all the engine subsystems, the concentrator, which is responsible for gathering and focusing the solar radiation, is regarded as a key element for the development of this propulsion technology [8]. It is also regarded as a promising research field due to the possible applications, such as communications, optical systems and electrical power generation [8].

The present project aims to complement and continue TU Delft's research lines by designing an inflatable concentrator tailored for a PocketQube (see Figure 1). This main task involves the development of the required design and analysis tools, the experimental demonstration and the analysis of the design of a concentrator meant for application to an *STP* engine.

This paper is organised in the same order of the steps taken in the research. The main requirements and the concept selection are described in chapter 2, followed by, firstly, the description of the design strategy and the modelling tools employed (section 3) and, secondly, the design results (section 4). The experimental phase, including the manufacturing and testing of the demonstrator, is described in section 5. As the main application conceived for this

DOI: 10.13009/EUCASS2017-438

concentrator, a preliminary design of an *STP* engine is made and benchmarked against existing systems in section 6. Finally, conclusions and recommendations are presented in section 7.

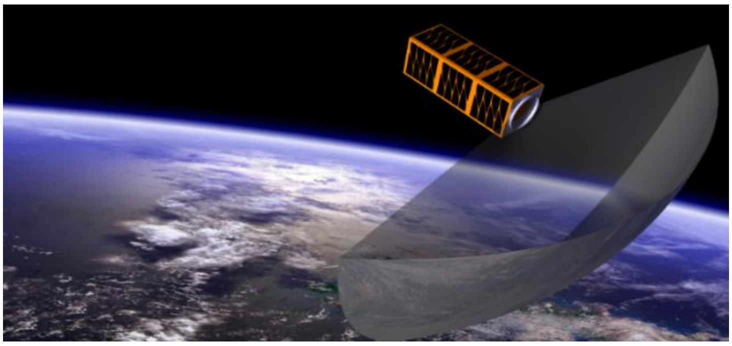

Figure 1: Artistic impression of the Concentrator during operation (a cross section view is presented for better understanding)

2. Design requirements and Concept Selection

The main design requirements and their rationales are described in this section, followed by the concept selection approach followed and its results.

2.1. Design requirements

The evaluation of the market needs and the characteristics of small satellites allowed to derive the design requirements. Table 1 presents the main design driver requirements together with their rationales. Further information about the justification of the requirements selected can be found in [8].

Table 1: Main design requirements and rationales

Requirement	Rationale
The Concentrator shall have a volume in the range of 0.5 to 1 *PQ* Unit (5x5x5 cm^3).	Balance between impact on the volume budget and power requirements.
The thermal power provided by the concentrator shall be ≥ 190 W at a distance of 1 AU from the Sun.	Value based on an *STP* engine running on NH_3 with a thrust of 100 mN and I_{sp} = 200 s.
The concentrator surface shall have an *rms*[1] error ≤0.5 mm for communications and optical applications and ≤7.5 mm for thermal power purposes	Even though a low *rms* error is not a strict requirement for *STP*, it would make the design also suitable for antenna and optical systems.
The concentrator shall be able to operate within an angular deviation of up to ±5 [deg] from the nominal orientation.	Angular range to mitigate the impact on the ADCS[2] of a small satellite.
The system shall have a lifetime of 1 year.	Usual duration of small satellite missions.

2.2. Concept Selection

A previous literature research performed on concentration devices applied to both space and ground purposes allowed to identify suitable solutions for the project objectives. The different concepts evaluated are described below, each of them with a corresponding identification label specified between parentheses.

[1] root-mean-square
[2] Attitude Determination and Control Subsystem

DOI: 10.13009/EUCASS2017-438

- On-axis (CS-I-ON) inflatable concentrator: thin-membrane device which attain the desired shape after being pressurised using gas [9] [10].
- Deployable Membrane Reflector (CS-M-A): concept based on the employment of membrane materials rigidized by a support structure which is deployed in orbit. It is similar to the Astromesh® system developed by Northrop Grumman [11].
- Rigid reflectors (CS-R): conventional concept used for communication purposes. They can be made of a single piece or multiple sections which are assembled in orbit, as the main reflector of the James Webb Space Telescope [12].

Rigid reflectors usually exhibit the highest optical performance due to the fact that their shape accuracy is still not attainable by the other two concepts. Even though the performance of membrane and inflatable concentrators is limited, there are already applications of membrane reflectors for communications and the research on inflatable structures is taking big steps towards their application in space systems. The interest on inflatable devices is mainly because of their low packaging volume, which makes them perfectly suitable for small spacecraft. Next to the above two factors, others such as simplicity, measured as the ease of deployment and the number of components required, and concept maturity, evaluated depending on the existence of previous applications to small satellites, need to be considered.

The concepts are traded on above criteria using an Analytical Hierarchical Process (or *AHP*), a strategy to compare different options according to a set of criteria (or *SC*) which depend on their relative relevance (see [8] for more information about the strategy and the results). The first step of this strategy consists in the definition of a relative weights matrix (Figure 2, left). The eigenvector associated to the highest eigenvalue of the matrix defines the weights to be used in the Pugh matrix (Figure 2, right). The weight factors and the results obtained were discussed with more experienced researchers to validate the selection process. Selection criteria included (1) aperture to packaging ratio, (2) optical performance and shape accuracy, (3) simplicity and (4) maturity of the concept.

	SC-1	SC-2	SC-3	SC-4
SC-1	1	2	3	4
SC-2	1/2	1	3/2	3
SC-3	1/3	2/3	1	3/2
SC-4	1/4	1/3	2/3	1

SC	Weight	CS-I-ON	CS-M-A	CS-R
SC-1	0.7798	2	1	-1
SC-2	0.5352	1	2	2
SC-3	0.2676	1	-1	1
SC-4	0.1838	1	0	2
	Result:	2.5462	1.5826	0.9258
	Weighted Result:	1	0.62155	0.3636

Figure 2: Selection criteria weights as a result of the AHP (left) and Pugh Matrix (right)

Based on the trade-off results (see Figure 2, right), the on-axis inflatable concept was chosen as the most suitable one. Its outstanding aperture to packaging volume ratio is decisive in this trade-off. Its poorer optical performance, however, is a point of concern that is tackled later in this work.

A schematic view a fully deployed on-axis inflatable concentrator applied on a 3-Unit *PQ* is shown in Figure 3. It consists of a reflective parabolic section and a conical transparent canopy. Solar radiation passes through the canopy, after which it hits the parabolic element and is reflected back towards the receiver. This latter element is located at the satellite wall, facing the reflector and perpendicular to its main axis. Other elements (not shown in the figure) include a pressurisation system in charge of ejecting the concentrator from the storage container and inflating it.

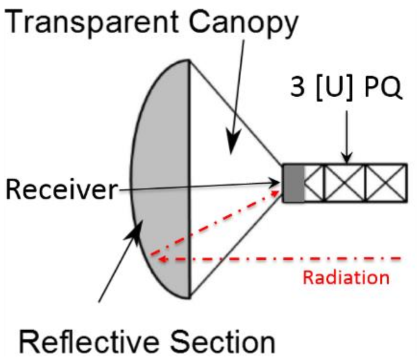

Figure 3: Sketch of the concept selected

DOI: 10.13009/EUCASS2017-438

3. Design Approach

In order to tackle the analysis of the selected concept and to obtain a more detailed design which fulfils the requirements previously introduced, an iterative design approach has been developed. This strategy involves using different models and is schematically depicted in Figure 4. In this approach, an initial ideal geometry is generated using a ray tracing tool. At this point, it is assumed that no deformations in the concentrator occur (hence the term ideal geometry) and the only non-nominal condition is given by the orientation of the solar rays. Next, the thermal and structural models are used to determine the shape error resulting from the loading conditions during operation. Thirdly, the ray tracing model is applied again to determine the effect of the thermal load and the deformations on the system's performance. Finally, the design is optimised by maximising the thermal output by reducing the *rms* error. The algorithm is repeated as many times as needed to meet the requirements. Following sections of this chapter describe the different modules the algorithm comprises.

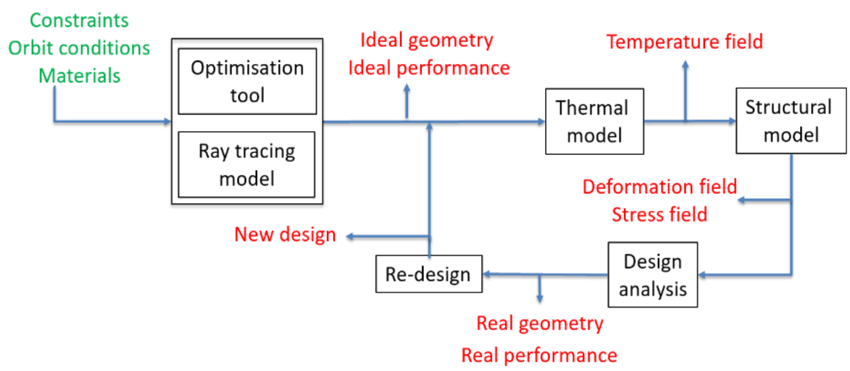

Figure 4: Design Algorithm

The design is developed assuming a set of nominal conditions which are presented hereafter:

- The concentrator is operating in a Low Earth Orbit (or *LEO*) around the Earth at an altitude of 600 km.
- The only radiation source considered is the Sun, assumed to be at a constant distance of 1 AU.
- The Solar rays are collimated.
- The Solar radiation is constant and equal to 1414 W/m^2.
- Under nominal conditions, the solar radiation is parallel to the main axis of the concentrator. Any deviation is measured with respect to this position.

3.1. Optical design

The optical design is performed using a ray tracing algorithm. The model provides the thermal power reflected onto the receiver as a function of the reflector's shape, the properties of the reflector coating and the transparent canopy and the illumination conditions (solar flux and relative orientation between the solar rays and the main axis of the concentrator). Using a grid of points as the origins of the rays, the algorithm follows the path described up to the reflector and, in case of impact, back to the receiver's plane. Figure 5 presents the ray tracing results of both a 2-D and a 3-D simulation. It is possible to observe how the rays converge on a point over the receiver's plane.

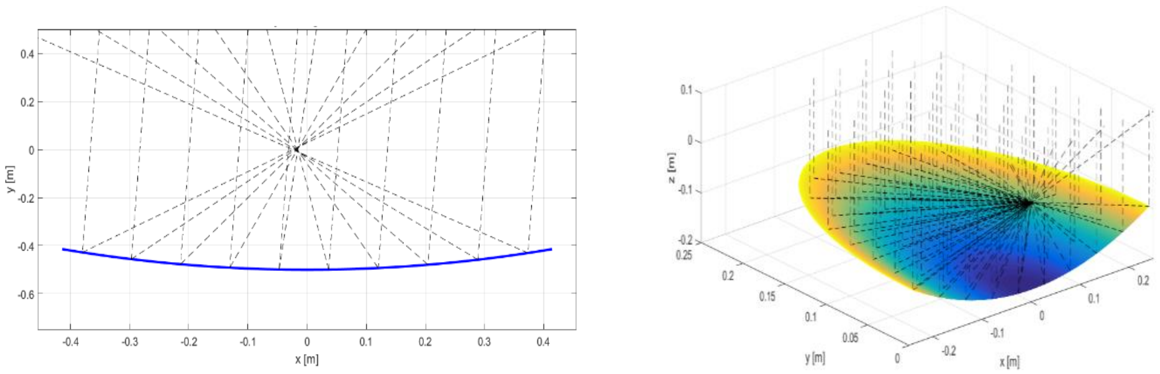

Figure 5: Results of the 2-D (left) and 3-D (right) ray tracing algorithms

DOI: 10.13009/EUCASS2017-438

The integration of the solar power arriving at the receiver gives the total thermal power collected. The analysis of the impact distribution over the plane allows evaluating how efficient the system reflects the incoming radiation (see Figure 6, left). As observed, the majority of the rays impact the plane within the receiver's area (defined by the black circle). It is also possible to derive the energy flux distribution (see Figure 6, right). The spot generated exhibits an energy flux which decreases rapidly as we look away from its centre. The thermal efficiency of the device benefits from high flux values due to the minimisation of the heat loses but thermal stresses may arise and that should be investigated. Similar results can be obtained to study the influence of the orientation of the incoming solar radiation.

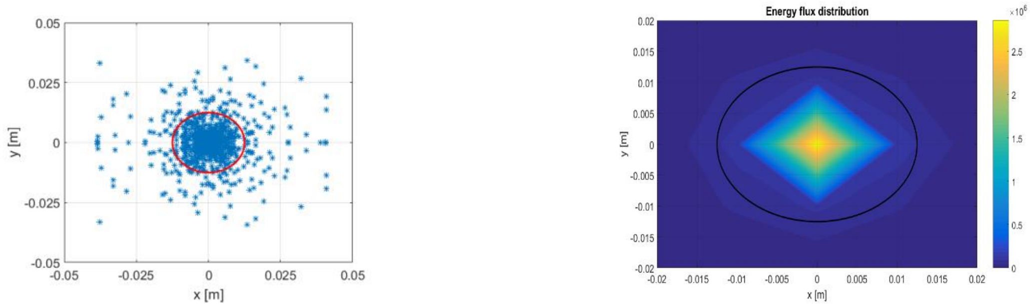

Figure 6: Impact distribution (left) and Energy Flux distribution (right) over the receiver's surface

The ideal geometry is generated by maximising the output thermal power. Given a packaging volume, it is possible to derive the maximum aperture attainable for a certain focal length. The effect of the direction of the solar radiation is taken into account by including in the target function the average thermal power over the angular deviation specified by the requirements.

3.2. Thermal design

The thermal model allows for estimating the temperature distribution over the reflector surface. For this purpose, an *FEM* is generated and the heat balance equations (1) and (2) are solved for each node « i » and its adjacent nodes « j » [13]. The first equation (1) implies that the difference between the incoming and emitted power equals the variation in the energy stored by the node. The second equation (2) defines the emitted power as the exchanged power by means of conduction (first term to the left of the equal sign) and radiation (last term of the equation).

$$Q_{in,i} - Q_{out,i} = m_i C_{p,i} \frac{\delta T_i}{\delta t} \tag{1}$$

$$Q_{out,i} = \sum_{j} C_{i,j} \cdot (T_i - T_j) + \sum_{j \neq i} B_{i,j} A_i \epsilon_i \sigma \cdot (T_i^4 - T_j^4) \tag{2}$$

An example of the temperature distribution is depicted in Figure 7. As observed, the nodes in front of the receiver and surrounding it are the ones reaching the highest temperatures. The gap seen in the geometry between the reflective section and the canopy is due to the discretisation limits of MATLAB®. The maximum temperature differences observed are in the order of 20 K, with the receiver's temperature over 1000 K.

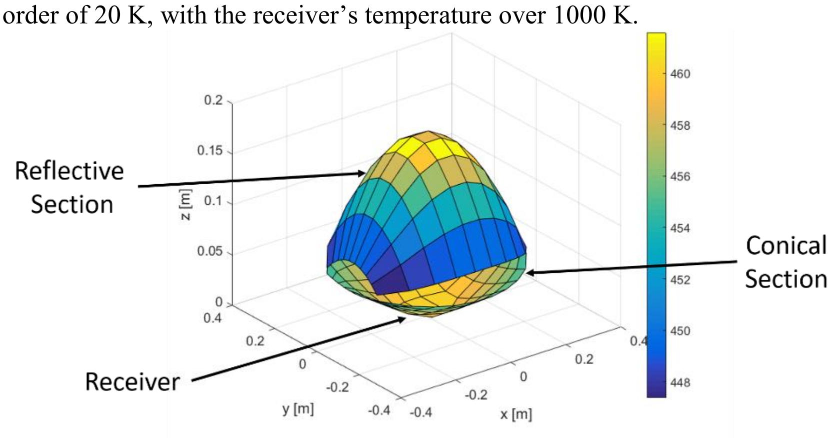

Figure 7: Example of the temperature distribution computed by the thermal model (in K)

DOI: 10.13009/EUCASS2017-438

The thermal model was verified using the experimental results obtained by Stegman et al. [11]. Figure 8 presents the temperature distribution estimated by the model used for this project (left) against the measurements presented in [11]. A maximum error of 17 K, which is translated into a difference in the order of 13%, is obtained. The reasons for possible remaining errors are that the materials properties are not well defined in [11] and the structure tested during test campaign is an Astromesh™ reflector, which comprises other elements -such as struts and cables- which are not taken into account in the model generated using the tool developed in this study.

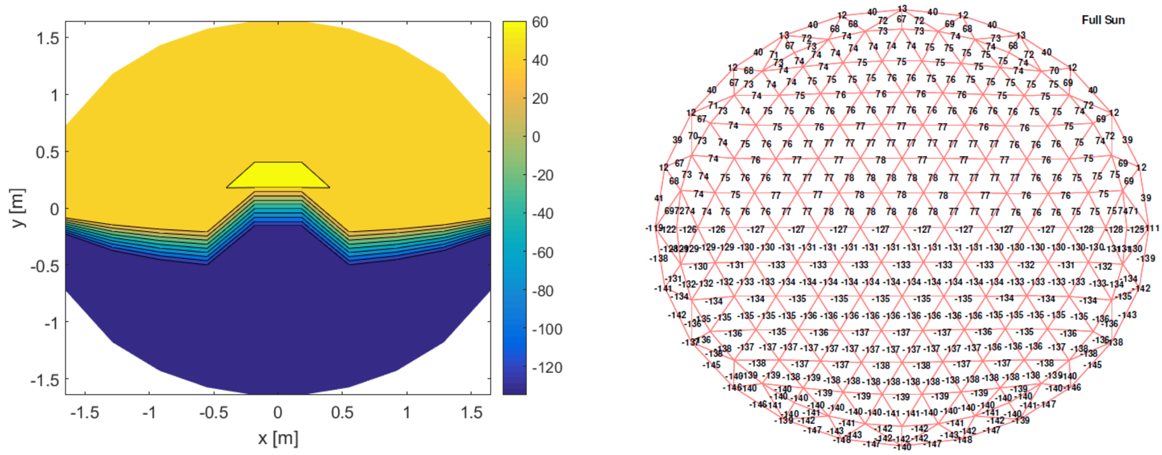

Figure 8: Results of the Thermal Model developed for this project (left) and temperature measurements obtained by Stegman et al. [11] (right)

3.3. Structural design

The structural design is performed using ANSYS. This tool allows to simulate the operational conditions with the intention of deriving the deformations and stresses on the structure. The applied loads consisted in the inflation pressure, defined as a design point, and the thermal loading obtained from the thermal model.

A typical output of the model is given in Figure 9. The *rms* and the locations of the maximum stress and the stress gradient are estimated from the deformation and stress fields, respectively. The joint connecting both sections of the reflector is the most critical area in terms of stress gradient; hence special attention must be given to this region during the production phase. The shape error (*rms* error) increases with pressure and with more severe thermal loads (larger temperature differences). This last effect is observed in the final design by an increase in the *rms* error from 0.13 mm to 0.48 mm. Contrary to the wrinkles around the edge, which are present if only the pressure load is applied, the formation of wrinkles over the two sections are triggered by the temperature differences.

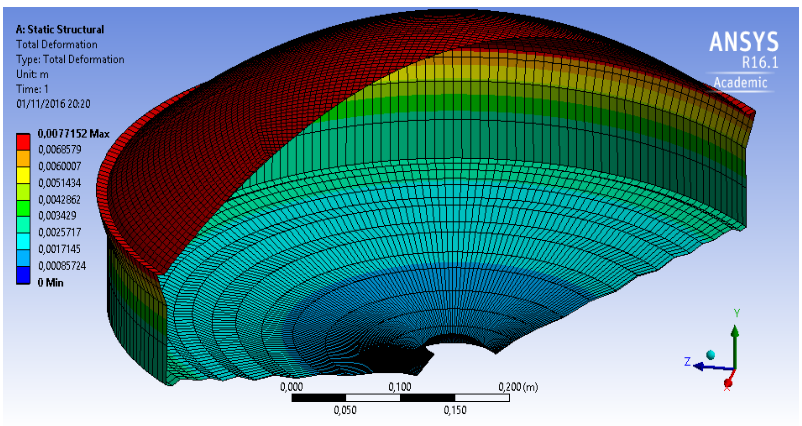

Figure 9: Deformation field over the concentrator

DOI: 10.13009/EUCASS2017-438

3.4. Design Optimisation

The design resulting from the analysis presented in the foregoing may present an *rms* error too high according to the design requirements. In fact, the structure resulting from the first iteration presents an *rms* error of 7.2 mm under nominal operational conditions. The optimisation module allows to optimise the power output and the imaging quality by reducing the *rms* shape error. Hence, a more accurate (the geometry is closer to the ideal one), stable (the device is less affected by changes in the incoming radiation) and versatile (the system can be applied to a broader range of applications) system is developed.

The optimisation approach consists in the application of changes in (1) focal length, (2) thickness and/or (3) concentrator height (defined as the distance from the vertex of the reflective section to the base of the canopy). The resulting geometry is re-analysed with the structural and optical models, assuming that no significant changes in the temperature distribution happen. A modification of the concentrator height is chosen as the most effective mitigation strategy based on the results (see [8] for more detailed data), leading to a final *rms* error of 0.48 mm.

4. Design Results

Based on the requirements stated in section 2, a parabolic on-axis inflatable reflector with a focal length of 0.175 m and an aperture of about 0.58 m has been designed. As membrane materials, Aluminised Mylar™ and Clear Mylar™ Type D with a thickness of 23 microns were selected for the parabolic and conical sections, respectively. These materials were selected given their suitable mechanical and thermal properties and their extensive availability. Figure 10 presents a schematic view of the reflector and its main dimensions.

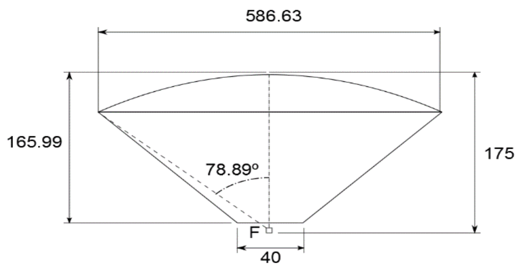

Figure 10: Main geometrical parameters of the final design

The system provides 232 W of thermal power under nominal conditions, which represents an efficiency of 60.73%. The losses are mainly due to materials properties (28 %), such as transmissivity, absorptivity and reflectivity, and the shape error (11.27 %). An *rms* error of 0.48 mm is derived from the structural analysis under the worst thermal case and an inflation pressure of 10 Pa. Table 2 includes the main results parameters. Further and more detailed information can be found in [8].

Table 2: Main parameters of the final design

Parameter	Value	Unit
Focal length	175	[mm]
Aperture half angle	79.89	[deg]
Aperture	586.6	[mm]
Film thickness	23	[µm]
rms error	0.48	[mm]
Power Output	230	[W]
Efficiency	60.7	[%]
Inflating pressure	10	[Pa]
Packaging Volume	1	[U]

A sensitivity analysis is performed to estimate the effect of changes in the concentrator height, inflation pressure, focal length and membrane thickness on the thermal output power. As observed in Table 3, the concentrator performance

DOI: 10.13009/EUCASS2017-438

has a low sensitivity (below 5%) to variations in concentrator height and inflation pressure, whereas the changes are larger for the other two parameters (well above 5%). Nevertheless, it must be pointed out that the design has been optimised for a given design point and, therefore, deviations are expected to affect the performance. This analysis unveils the relevance of the manufacturing accuracy and it can be used to set requirements on the design of auxiliary systems, such as the deployment mechanism.

Table 3: Results of the sensitivity analysis

Parameter	Nominal Value	Value A	ΔP [%]	Value B	ΔP [%]
Focal length	175 [mm]	180 [mm]	-1.33	170 [mm]	-11.87
z_{rec}	-0.15 [mm]	0.85 [mm]	-0.51	-1.15 [mm]	-3.30
Thickness	23 [μm]	50 [μm]	-35.27	19 [μm]	-9.80
Pressure	10 [Pa]	11 [Pa]	-0.53	9 [Pa]	-2.87

An issue which must be investigated in relation with the application of inflatable structures in space systems is the risk of micrometeoroid impacts and the subsequent pressure loss. The device relies on the pressurising gas to maintain its shape at a given pressure. Therefore, any leak would cause shape errors and a decrease in performance. The estimations performed within this project assume that (1) the pressurisation system uses nitrogen, (2) the micrometeoroid and space debris density corresponds to the one provided by SPENVIS [14] for an altitude of 600 km, (3) the pressure losses are due to the impacts and the materials' permeability, (4) any leak due to impacts is modelled as a choked flow and (5) the formation of holes in the membrane materials as a result of impacts depends on the ratio between the size of the object and the thickness of the structure following the model published by Grossman and Williams [15]. This results in a total pressurising mass loss of 29.9 g after a 1-year mission. Considering the micro cool gas generators used for Delfi n3Xt Cubesat [16], the lifetime of the system would be limited to 22 days. Longer lifetimes could be attained by increasing the thickness, decreasing the inflation pressure or using another pressurising gas with a higher molar mass, such as benzoic acid.

5. Test Campaign

Following the design of the concentrator, an experimental campaign has been set up and carried out using a small scale demonstrator to verify and validate the design approach devised.

5.1. Manufacturing

The small scale demonstrator was designed using the approach described in section 3. Its main characteristics are given in Table 4 in comparison with the flight system designed earlier. The size of the test item was chosen mainly due to two reasons: (1) the material availability and (2) the dimensions of the spot generated by the light source used in this test campaign. Kenpro™ mirror film and clear Mylar™ Type A were used as film materials and were supplied by *Lohmann Technologies UK*. The device was inflated using CO2 cartridges, as a low cost solution based on COTS[3] components.

Table 4: Comparison between the design parameters of the flight system and the demonstrator

Parameter	Flight System	Demonstrator	Unit
Focal length	175	167	[mm]
Aperture half angle	79.89	53.37	[deg]
Aperture	586.6	335.2	[mm]
Film thickness	23	23	[μm]

The theoretical performance of the demonstrator in conjunction with the non-collimated artificial light source used (see the following subsection) is estimated in the range of 14 to 21 W of collected thermal power which results in an efficiency of about 16 to 22 %. This low thermal output range is due to the low quality of the light source and the thermal properties of the film materials (transmissivity, emissivity, absorptivity and reflectivity).

[3] Commercial-Off-The-Shelf

DOI: 10.13009/EUCASS2017-438

A petal-based approach was used to manufacture the device, using Kapton™ tape as the joining material. The petals were designed such that the assembled structure resembles the paraboloid with the desired geometry (see Figure 11). Other procedures, such as one-shot casting, would provide a better shape accuracy but at a higher cost and requiring more specialised instruments. In this case, only a cutting knife, Kapton™ tape and moulds were required.

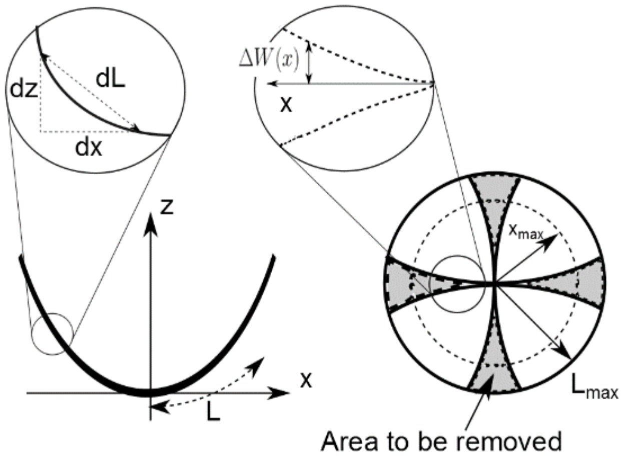

Figure 11: Petal-based manufacturing approach

Figure 12 shows the resulting structure after assembling it on the test set-up and after completing the pressurisation sequence. Visual inspections before and after inflation unveiled large irregularities and shape errors, which need addressing in future to allow the production of a more optimum demonstrator. It was also found that special attention must be given to the cutting and joining methods to reduce the shape error and to prevent deflation.

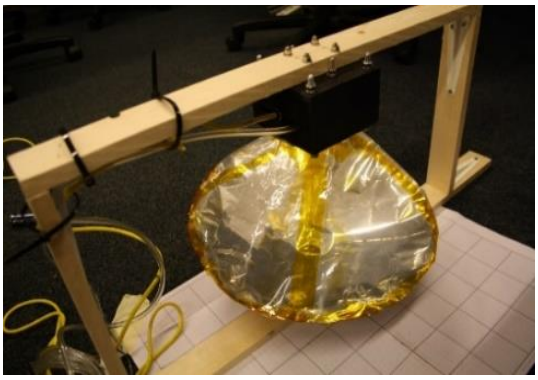

Figure 12: View of the demonstrator after inflation

5.2. Test Phase

In order to eliminate the dependency on weather conditions, an artificial, low cost, non-collimated light source (theatre lamp) was employed for the test campaign. Tests with the lamp were performed to determine the radiative flux distribution emitted by the lamp (see Figure 13 for the average heat flux measured during the tests). Test results showed that the flux density varies between a maximum of about 2500 W/m^2 at the centre and a minimum value of 20 W/m^2 at a distance of 55 cm (in radial direction) from this position. By integrating the flux density measurements over the concentrator aperture area, the total thermal power arriving at the area of interest is estimated at ~100 W. The results unveiled instabilities causing flux variations in time and direction, with deviations in the order of 5% with respect to the average flux value at each position.

DOI: 10.13009/EUCASS2017-438

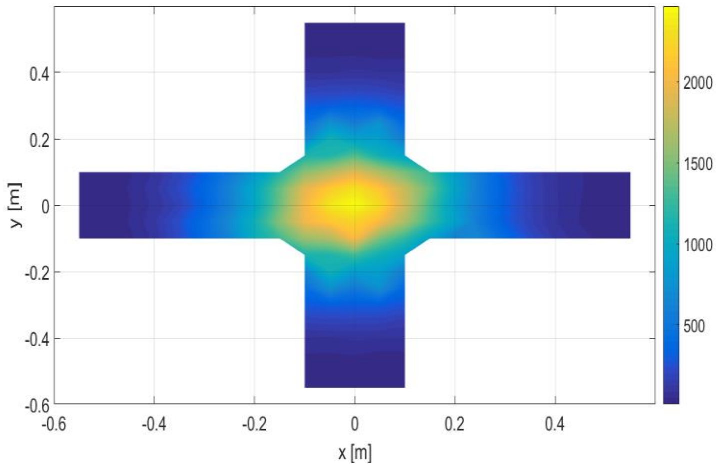

Figure 13: Average irradiance (in W/m^2) emitted by the lamp measured over a plane located at 1.6 m from the source

The demonstrator was inflated and exposed to the light source radiation. The concentrator is placed as indicated in Figure 12 and Figure 14 (left). The lamp is mounted vertically and aligned with the main axis of the small-scale demonstrator at a distance of 1.6 m (measured between the vertex of the reflective section and the lamp). The reflected thermal output was measured with a pyranometer connected to a multimeter. The interface element (see Figure 14, right) was designed to mount the demonstrator, seal its interior and to hold the pyranometer and the connections of the feed system. It was 3D printed to lower the production cost.

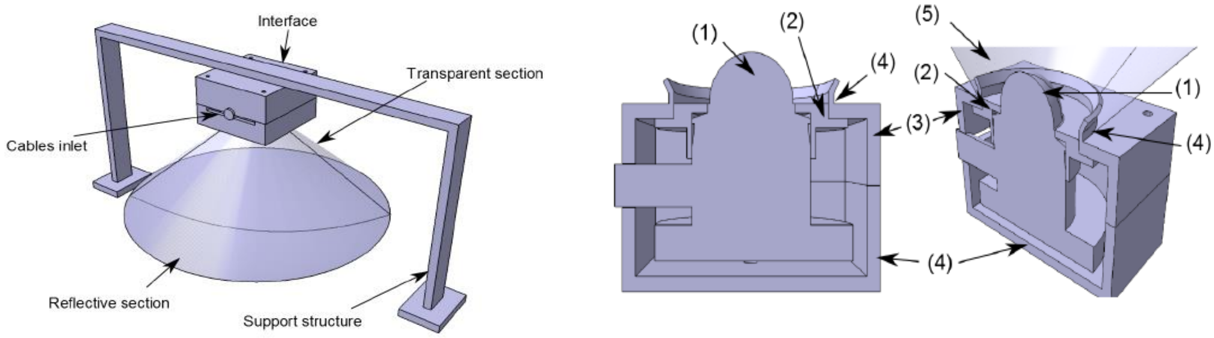

Figure 14: Main view of the demonstrator assembly (left) and detailed view of the interface element designed to connect the concentrator and the set-up (right). The latter figure includes: figure includes (1) the pyranometer, (2) the sealing ring, (3) the interface upper side, (4) the interface rear side and (5) the concentrator.

The test of the small scale yielded an efficiency in the range 4- 6 %. This is much lower than the theoretical predicted values (~16-22 %). See Table 5 for further results. The differences are mainly due to both the irregular shape of the concentrator and the uncertainty in the radiation emitted by the lamp, which are key inputs for the ray tracing algorithm. Nevertheless, the concept is demonstrated to be feasible and it has the potential to provide a better performance if the recommendations on the production and testing phases are applied.

Table 5: Theoretical and Experimental efficiency values for the different test cases

Test case	Theoretical Efficiency [%]	Measured Efficiency [%]
TEST-1	22.33	4.86
TEST-2	22.33	4.69
TEST-3	16.74	5.81

DOI: 10.13009/EUCASS2017-438

6. Solar Thermal Propulsion Engine

The potential performance of an *STP* engine has been analysed to demonstrate its promising capabilities. To this end, an engine with a flat receiver/heat exchanger with integral fluid channels (see Figure 15) connected to a convergent-divergent nozzle has been devised. Propellant is fed through the channels to the exchanger, where it is heated up to a high temperature by using the gathered solar radiation. The fluid is then expanded in the nozzle to produce the thrust. The flat receiver/heat exchanger is placed in the focal plane of the concentrator with the largest side facing the radiation.

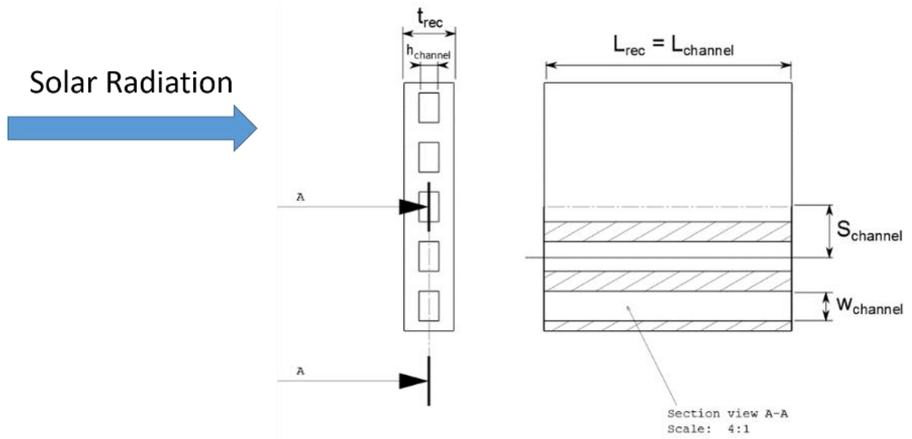

Figure 15: Flat heat exchanger

A design model of the engine has been developed comprising a thermal and a propulsive sub-module. The former determines the amount of thermal power transmitted to the fluid through forced convection as well as the propellant exhaust temperature just before entering the nozzle. The latter computes the propulsion capabilities of the system, including parameters such as thrust (F), specific impulse (I_{sp}) and thrust efficiency (η_T). The model allows determining the performance while varying design parameters such as the number of fluid channels ($n_{channel}$), the channel's cross-section ($h_{channel} \cdot w_{channel}$), the propellant properties and the mass flow rate ($\dot{m}$). Other relevant variables derived from the model are the receiver efficiency (η_{rec}) and the throat to exhaust area ratio of the nozzle (A_e/A_T).

A design has been made considering Ammonia as the propellant and assuming a received input power of 222.76 W. The selection of Ammonia is due to its storability properties at room temperature, non-toxicity and availability. Nevertheless, it is also chosen because it has already been considered for *STP* applications, which makes the model verification easier, and it is a propellant commonly used in the industry. Others propellants, such as hydrogen, may be considered for a higher performance.

The resulting design provides a thrust level of 160 mN and a specific impulse of 200 s with a 5-channel configuration. Hot ammonia temperature is in the order of 900 to 1000 K. Considering that the engine has a total volume of 1.5 *PQ*, which equals 187.5 cm^3, the thrust to volume ratio of the entire system results in 0.87 mN/cm^3. The end-to-end efficiency of the system is computed using the ratio between the propellant exhaust power ($P_J = 0.5 \cdot F^2/\dot{m}$) and the input thermal power arriving at the concentrator (382.18 W). This results in an efficiency of about 43 %. More design details can be found in Table 6. These values are in the same order as those obtained in similar projects related to *STP* [7] [17].

Table 6: Design and performance parameters of the STP engine

Parameter	Value	Unit
$\dot{m}$	80	[mg/s]
$n_{channel}$	5	[mm]
$h_{channel}$	0.3	[mm]
$w_{channel}$	2.5	[mm]
η_{rec}	75.91	[%]
A_e/A_T	18.76	[-]
I_{sp}	206.91	[s]

DOI: 10.13009/EUCASS2017-438

Parameter	Value	Unit
F	162.4	[mN]
η_T	66.63	[%]
Volume	1.5	[U]
Input Power	222.76	[W]
Total efficiency	43	[W]
F/V	0.87	[mN/cm^3]

When benchmarked with competing systems, the thrust to volume ratio is between solar electric (< 0.1 mN/cm^3) and chemical engines (> 1 mN/cm^3). Although the specific impulse is in the same order of chemical propulsion, it is expected that switching to other propellants (e.g. Hydrogen) would make a large difference due to the lower molecular mass and different thermal properties. Moreover, the advantages with respect to solar electric propulsion are not limited to the thrust to volume ratio but also lie in an end-to-end efficiency at least 3 times higher than solar electric engines. For further information about the benchmarking analysis, refer to [8].

7. Conclusions and Recommendations

In this project, an inflatable solar concentrator has been designed using an iterative approach. This strategy allows to optimise the shape of the collector to maximise the thermal performance thereby taking into account the effects of thermal and pressure loading and shape errors. The tool has demonstrated the ability to limit the *rms* shape error below 0.5 mm, thus showing the potential of the inflatable concentrator not only for Solar Thermal Propulsion, but also for other purposes such as communications or optical devices.

The design approach has been applied to an inflatable, on-axis, parabolic demonstrator tailored for a single *PQ* unit, but it could be also scaled to bigger spacecraft. Moreover, no showstopper has been found, which justifies continuing this research line due to the promising capabilities of the concept. Considering the high power collected and the small volume of the system in its stowed configuration, the concept is very suited for solar power collection purposes.

A small-scale demonstrator of the system has been designed, manufactured and tested. The experimental phase of the project showed that this demonstrator has the capability of reaching an overall energy efficiency of around 10% when exposed to a simple light source. Issues identified showed that special attention must be given to the manufacturing approach.

A first concept of an *STP* engine tailored for a *PQ* has been designed, resulting in a system whose performance capabilities exhibit relevant advantages compared to other non-*STP* technologies available in the market. The thrust to volume ratio and the end-to-end efficiency of the solar collector based system outperforms the capabilities so far exhibited by solar electric engines. Nevertheless, the promising theoretical results must be demonstrated in space. Therefore, the authors encourage researchers in the field to perform further research towards the application of *STP* to PocketQubes due to the technological and economic viability of the concept.

From the results also certain recommendations follow for improvement of the chosen concept. It is advised to research (1) other manufacturing approaches, such as laser cutting and continuous joining methods; (2) suitable materials with better optical properties so that the efficiency is increased; (3) different material thicknesses to make production easier and decrease the pressure loss due to micrometeoroid impacts; and (4) other inflation pressures, to limit the consequences of leakages. The effect of micrometeoroid impacts and the corresponding pressure loss is an issue that should be tackled to increase the lifetime of the system. Further recommendations include the modification of the set-up to have a more suitable light source and/or to adapt the models to better reproduce the shape errors and the input radiation. All these topics should be tackled to turn the design we present into a flight system with a performance more similar to the theoretical one.

DOI: 10.13009/EUCASS2017-438

References

[1] B. Doncaster, and J. Shulman, *2016 Nano/Microsatellite Market forecast*, SpaceWorks Enterprises, Inc., USA (2016)

[2] R. Sandau, K. Brieb and M. E'Errico, *Small Satellites for Global Coverage: Potential and limits*, ISPRS Journal of Photogrammetry and Remote Sensing, vol. 65 pp. 492-504, Elsevier (2010).

[3] Delft University of Technology, *The Delffi Space Project website* (www.delfispace.nl), last accessed on 10/01/2017

[4] Website of the Department of Space Engineering of Delft University of Technology (https://www.tudelft.nl/en/ae/organisation/departments/space-engineering/), last accessed on 10/01/2017.

[5] A. Cervone et al., *Green micro-resistojet research at Delft University of Technology: the new frontiers of CubeSat propulsion*, CEAS Space Journal, vol. 9, pp. 111-125, Springer (2016).

[6] H. C. M. Leenders and B. T. C. Zandbergen. *Development of a Solar Thermal Thruster System*, 59th IAC Congress, Scotland (2008).

[7] P. Henshall and P. Palmer, *Solar Thermal Propulsion Augmented with Fiber Optics: Technology Development*, 42nd AIAA/ASME/SAE/ASEE Joint Propulsion Conference And Exhibit, AIAA 2006-4874, American Institute of Aeronautics and Astronautics (2006).

[8] D. Martinez Pino, *Solar Concentrator Demonstrator for PocketQubes*, Master Thesis, TU Delft, The Netherlands (2016). Available for download via TU Delft repository (http://repository.tudelft.nl/)

[9] A. Babuscia et al. *Inflatable antenna for CubeSats: Motivation for development and antenna design*, Acta Astronautica vol. 91, pp. 322-332, Elsevier (2013).

[10] J. Pearson, J. Moore, and H. Fang. *Large and High Precision Inflatable Membrane Reflector, 51st AIAA/ASME/ASCE/AHS/ASC Structures*, Structural Dynamics and Materials Conference, AIAA 2002-3928, American Institute of Aeronautics and Astronautics (2010).

[11] M. Stegman, M. Fedyk and S. Kuehn, *Solar Thermal Vacuum Testing of Deployable Mesh Reflector for Model Correlation*, Aerospace Conference, 1497, IEEE (2010).

[12] C. Lillie, *Large Deployable Telescopes for Future Space Observatories*, Proceedings of SPIE, vol. 5889, SPIE (2015).

[13] R. D. Karam, *Satellite Thermal Control for Systems Engineers*, Progress in Astronautics and Aeronautics, vol. 181, AIAA (1998).

[14] *The Space Environment Information System* (SPENVIS), available on www.spenvis.oma.be, ESA Technical Officer. Last accessed on 10/01/2017.

[15] G. Grossman and G. Williams, *Inflatable Concentrators for Solar Propulsion and Dynamic Space Power*, Journal of Solar Energy Engineering, vol. 112/229, The American Society of Mechanical Engineers (1990).

[16] Delft University of Technology, *Delfi-n3xt micropropulsion payload*, available on http://www.delfispace.nl/delfi-n3xt/micropropulsion-payload. Last accessed on 08/05/2016.

[17] H. Sahara and M. Shimizu, *Solar Thermal Propulsion System for Microsatellite Orbit Transferring*, 40th AIAA/ASME/SAE/ASEE Joint Propulsion Conference And Exhibit, AIAA 2004-3764, American Institute of Aeronautics and Astronautics (2004).

[18] D. Martinez Pino, B. Zandbergen and O. Bergsma, *Design of a Solar Concentrator Demonstrator for PocketQubes*, 11th IAA Symposium on Small Satellites for Earth Observation, IAA-B11-1105P, International Academy of Astronautics (2017). Temporarily available under request on https://owncloud.tu-berlin.de/index.php/s/e8cwvJWI9UJ2vSm